Definition of the Floating System for Phase IV of OC3

Jason Jonkman

National Wind Technology Center (NWTC)
National Renewable Energy Laboratory (NREL)
1617 Cole Blvd.
Golden, CO. 80401-3393
United States of America
Phone: +1 (303) 384 – 7026
Fax: +1 (303) 384 – 6901
E-mail: jason_jonkman@nrel.gov

July 10, 2009

Table of Contents

List of Tables

List of Figures

1 Introduction

Phase IV of the IEA Annex XXIII Offshore Code Comparison Collaboration (OC3) involves the modeling of an offshore floating wind turbine. This report documents the specifications of the floating system, which are needed by the OC3 participants for building aero-hydro-servo-elastic models.

As in previous phases of the OC3 project, Phase IV uses the turbine specifications of the National Renewable Energy Laboratory (NREL) offshore 5-MW baseline wind turbine [7], which is a representative utility-scale multimegawatt turbine that has also been adopted as the reference model for the integrated European UpWind research program.[1] In Phase IV, the rotor-nacelle assembly of this 5-MW turbine—including the aerodynamic and structural properties—remains the same, but the support structure (tower and substructure) and control system properties have been changed.

Numerous floating platform concepts are possible for offshore wind turbines, including spar-buoys, tension leg platforms (TLPs), barges, and hybrid concepts thereof. Per the request of the OC3 participants, the spar-buoy concept called "Hywind," developed by StatoilHydro of Norway,[2] was chosen for the modeling activities of Phase IV. This concept was chosen for its simplicity in design, suitability to modeling, and propinquity to commercialization. Finn Gunnar Nielsen and Tor David Hanson of StatoilHydro were contacted and graciously supplied detailed platform and mooring system data. The data provided was for the conceptual version of the Hywind platform developed to support a 5-MW wind turbine, as analyzed by Nielsen, Hanson, and Skaare [11,12] and Larsen and Hanson [9]. Per the request of StatoilHydro, the originally supplied data has been condensed and sanitized by Jason Jonkman of NREL so that it is suitable for public dissemination. Aspects of the original data were also adapted slightly by Jason Jonkman so that the platform design is appropriate for supporting the NREL 5-MW baseline turbine, which has properties that are slightly different than the turbine properties used by StatoilHydro in their development of the system. The new system is referred to as the "OC3-Hywind" system in this report, to distinguish it from StatoilHydro's original Hywind concept.

This report presents the tailored data, as well as data that has been derived apart from that supplied by StatoilHydro but which is needed to support the activities of the OC3 project. The material is presented as follows:

- The tower properties in Section 2
- The floating platform structural properties in Section 3
- The floating platform hydrodynamic properties in Section 4
- The mooring system properties in Section 5
- The control system properties in Section 6

[1] Web site: http://www.upwind.eu/default.aspx

[2] Web site: http://www.statoilhydro.com/en/TechnologyInnovation/NewEnergyAndRenewables/Wind/VindTilHavs/Pages/Hywind.aspx

2 Tower Properties

The base of the tower is coincident with the top of platform and is located at an elevation of 10 m above the still water level (SWL). The top of the tower is coincident with the yaw bearing and is located at an elevation of 87.6 m above the SWL. This tower-top elevation—and the corresponding 90 m elevation of the hub above the SWL—is consistent with the land-based version of the NREL 5-MW baseline wind turbine (as given in Ref. [7]). These properties are all relative to the undisplaced position of the platform.

The distributed properties of the tower for the NREL 5-MW baseline wind turbine atop the OC3-Hywind spar-buoy are founded on the base diameter of 6.5 m, which matches the top diameter of the platform (see Section 3), and the tower base thickness (0.027 m), top diameter (3.87 m) and thickness (0.019 m), and effective mechanical steel properties of the tower used in the DOWEC study (as given in Table 9 on page 31 of Ref. [8]). The Young's modulus was taken to be 210 GPa, the shear modulus was taken to be 80.8 GPa, and the effective density of the steel was taken to be 8,500 kg/m^3. The density of 8,500 kg/m^3 was meant to be an increase above steel's typical value of 7,850 kg/m^3 to account for paint, bolts, welds, and flanges that are not accounted for in the tower thickness data. The radius and thickness of the tower are assumed to be linearly tapered from the tower base to tower top. Table 2-1 gives the resulting distributed tower properties.

Table 2-1. Distributed Tower Properties

Elevation (m)	HtFract (-)	TMassDen (kg/m)	TwFAStif (N•m^2)	TwSSStif (N•m^2)	TwGJStif (N•m^2)	TwEAStif (N)	TwFAIner (kg•m)	TwSSIner (kg•m)	TwFAcgOf (m)	TwSScgOf (m)
10.00	0.00000	4667.00	603.903E+9	603.903E+9	464.718E+9	115.302E+9	24443.7	24443.7	0.0	0.0
17.76	0.10000	4345.28	517.644E+9	517.644E+9	398.339E+9	107.354E+9	20952.2	20952.2	0.0	0.0
25.52	0.20000	4034.76	440.925E+9	440.925E+9	339.303E+9	99.682E+9	17847.0	17847.0	0.0	0.0
33.28	0.30000	3735.44	373.022E+9	373.022E+9	287.049E+9	92.287E+9	15098.5	15098.5	0.0	0.0
41.04	0.40000	3447.32	313.236E+9	313.236E+9	241.043E+9	85.169E+9	12678.6	12678.6	0.0	0.0
48.80	0.50000	3170.40	260.897E+9	260.897E+9	200.767E+9	78.328E+9	10560.1	10560.1	0.0	0.0
56.56	0.60000	2904.69	215.365E+9	215.365E+9	165.729E+9	71.763E+9	8717.2	8717.2	0.0	0.0
64.32	0.70000	2650.18	176.028E+9	176.028E+9	135.458E+9	65.475E+9	7124.9	7124.9	0.0	0.0
72.08	0.80000	2406.88	142.301E+9	142.301E+9	109.504E+9	59.464E+9	5759.8	5759.8	0.0	0.0
79.84	0.90000	2174.77	113.630E+9	113.630E+9	87.441E+9	53.730E+9	4599.3	4599.3	0.0	0.0
87.60	1.00000	1953.87	89.488E+9	89.488E+9	68.863E+9	48.272E+9	3622.1	3622.1	0.0	0.0

The entries in the first column, "Elevation," are the vertical locations along the tower centerline relative to the SWL. "HtFract" is the fractional height along the tower centerline from the tower base (0.0) to the tower top (1.0). The rest of columns are similar to those described for the distributed blade properties presented in Ref. [7].

The resulting overall (integrated) tower mass is 249,718 kg and is centered [i.e., the center of mass (CM) of the tower, is located] at 43.4 m along the tower centerline above the SWL. This result follows directly from the overall tower length of 77.6 m.

A structural-damping ratio of 1% critical is specified for all modes of the isolated tower (cantilevered atop a rigid foundation without the rotor-nacelle assembly mass present), which corresponds to the values used in the DOWEC study (from page 21 of Ref. [8]).

Table 2-2 summarizes the undistributed tower properties discussed in this section.

Table 2-2. Undistributed Tower Properties

Elevation to Tower Base (Platform Top) Above SWL	10 m
Elevation to Tower Top (Yaw Bearing) Above SWL	87.6 m
Overall (Integrated) Tower Mass	249,718 kg
CM Location of Tower Above SWL Along Tower Centerline	43.4 m
Tower Structural-Damping Ratio (All Modes)	1%

3 Floating Platform Structural Properties

The tower is cantilevered at an elevation of 10 m above the SWL to the top of the floating platform, which—for the purposes of analysis—is considered to be a rigid body. The draft of the platform is 120 m. Between the top and bottom of the platform, the OC3-Hywind spar-buoy consists of two cylindrical regions connected by a linearly tapered conical region. The cylinder diameter of 6.5 m above the taper is more slender than the cylinder diameter of 9.4 m below the taper to reduce hydrodynamic loads near the free surface. The linearly tapered conical region extends from a depth of 4 m to a depth of 12 m below the SWL. These properties are all relative to the undisplaced position of the platform.

The mass, including ballast, of the floating platform is 7,466,330 kg. This mass was calculated such that the combined weight of the rotor-nacelle assembly, tower, and platform, plus the weight of the mooring system (not including the small portion resting on the seafloor) in water, balances with the buoyancy (i.e., weight of the displaced fluid) of the undisplaced platform in still water. This mass is centered [i.e., the CM of the floating platform, including ballast, is located] 89.9155 m along the platform centerline below the SWL, which was derived so as to ensure that the CM location of the full system (turbine plus platform) matched that specified in the data supplied by StatoilHydro. The roll and pitch inertias of the floating platform about its CM are 4,229,230,000 kg•m^2 and the yaw inertia of the floating platform about its centerline is 164,230,000 kg•m^2. These inertias were calculated using a mass distribution appropriate to the floating platform. The inertias of the full OC3-Hywind system are higher than those of StatoilHydro's Hywind system because the NREL offshore 5-MW baseline wind turbine is heavier than the turbine in StatoilHydro's Hywind system.

Table 3-1 summarizes the undistributed tower properties discussed in this section and Figure 3-1 illustrates the concept with an image generated using MSC.ADAMS.

Table 3-1. Floating Platform Structural Properties

Depth to Platform Base Below SWL (Total Draft)	120 m
Elevation to Platform Top (Tower Base) Above SWL	10 m
Depth to Top of Taper Below SWL	4 m
Depth to Bottom of Taper Below SWL	12 m
Platform Diameter Above Taper	6.5 m
Platform Diameter Below Taper	9.4 m
Platform Mass, Including Ballast	7,466,330 kg
CM Location Below SWL Along Platform Centerline	89.9155 m
Platform Roll Inertia about CM	4,229,230,000 kg•m^2
Platform Pitch Inertia about CM	4,229,230,000 kg•m^2
Platform Yaw Inertia about Platform Centerline	164,230,000 kg•m^2

In the sections that remain, several of the platform specifications refer to an inertial reference frame and platform degrees of freedom (DOFs). In these sections, *X*,*Y*,*Z* represents the set of orthogonal axes of this reference frame, with the *XY*-plane designating the SWL and the *Z*-axis directed upward opposite gravity along the centerline of the undisplaced platform. The rigid-body platform DOFs include translational surge, sway, and heave motions and rotational roll,

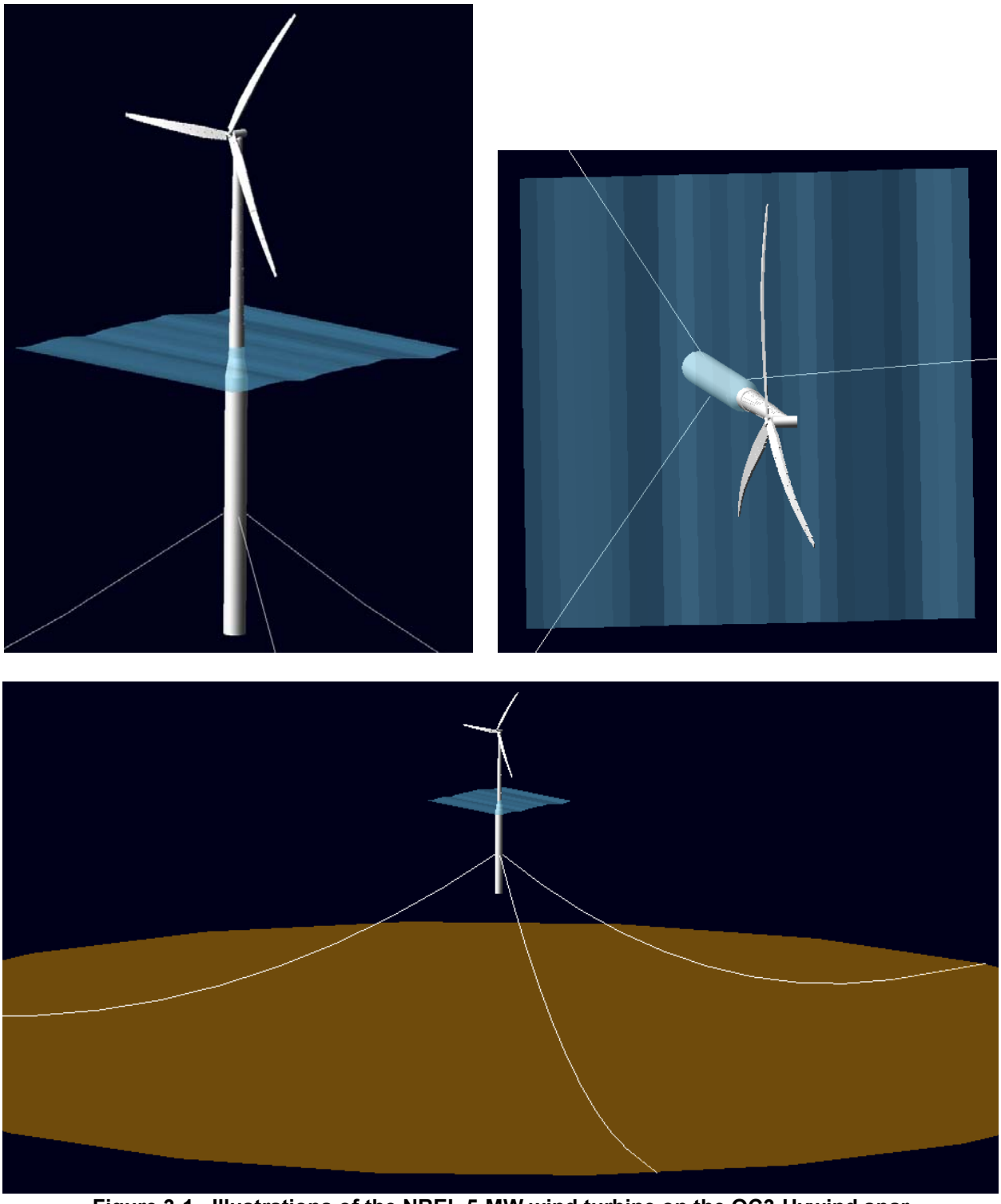

Figure 3-1. Illustrations of the NREL 5-MW wind turbine on the OC3-Hywind spar

pitch, and yaw motions. Positive surge is defined along the positive *X*-axis, sway is along the *Y*-axis, and heave is along the *Z*-axis. Positive roll is defined about the positive *X*-axis, pitch is about the *Y*-axis, and yaw is about the *Z*-axis.

4 Floating Platform Hydrodynamic Properties

Hydrodynamic loads include contributions from linear hydrostatics, linear excitation from incident waves, linear radiation from outgoing waves (generated by platform motion), and nonlinear effects. The linear hydrostatic properties of the floating platform are presented first; presentation of the remaining properties follows.

The total load on the floating platform from linear hydrostatics, $F_i^{Hydrostatic}$, is

$$F_i^{Hydrostatic}(q) = \rho g V_0 \delta_{i3} - C_{ij}^{Hydrostatic} q_j , \tag{4-1}$$

where ρ is the water density, g is the gravitational acceleration constant, V_0 is the displaced volume of fluid when the platform is in its undisplaced position, δ_{i3} is the (i,3) component of the Kronecker-Delta function (i.e., identity matrix), $C_{ij}^{Hydrostatic}$ is the (i,j) component of the linear hydrostatic-restoring matrix from the effects of water-plane area and the center of buoyancy (COB), and q_j is the j^{th} platform DOF. (Without the subscript, q represents the set of platform DOFs. $F_i^{Hydrostatic}$ depends on q as indicated.) In Eq. (4-1), subscripts i and j range from 1 to 6; one for each platform DOF (1 = surge, 2 = sway, 3 = heave, 4 = roll, 5 = pitch, 6 = yaw). Einstein notation is used here, in which it is implied that when the same subscript appears in multiple variables in a single term, there is a sum of all of the possible terms. The loads are positive in the direction of positive motion of DOF i. Equation (4-1) does not include the restoring effects of body weight (i.e., gravitational restoring). Instead, the gravitational restoring is assumed to be included within the structural dynamics models.

The first of the terms on the right-hand side of Eq. (4-1) represents the buoyancy force from Archimedes' principle; that is, it is the force directed vertically upward and equal to the weight of the displaced fluid when the platform is in its undisplaced position. This term is nonzero only for the vertical heave-displacement DOF of the support platform (DOF i = 3) because the COB lies on the centerline of the undeflected tower. The second of the terms on the right-hand side of Eq. (4-1) represents the change in the hydrostatic force and moment as the platform is displaced. The formulation for $C_{ij}^{Hydrostatic}$ in terms of a platform's water-plane shape, displaced volume, and COB location is given in Ref. [5].

The water density is chosen to be 1,025 kg/m^3. From the external geometry of the floating platform, then, $\rho g V_0$ and $C_{ij}^{Hydrostatic}$ were calculated to be:

$$\rho g V_0 = 80{,}708{,}100\ N \tag{4-2}$$

and

$$C_{ij}^{Hydrostatic} = \begin{bmatrix} 0 & 0 & 0 & 0 & 0 & 0 \\ 0 & 0 & 0 & 0 & 0 & 0 \\ 0 & 0 & 332{,}941\ N/m & 0 & 0 & 0 \\ 0 & 0 & 0 & -4{,}999{,}180{,}000\ Nm/rad & 0 & 0 \\ 0 & 0 & 0 & 0 & -4{,}999{,}180{,}000\ Nm/rad & 0 \\ 0 & 0 & 0 & 0 & 0 & 0 \end{bmatrix}. \quad (4\text{-}3)$$

The roll-roll (*4*,*4*) and pitch-pitch (*5*,*5*) elements of $C_{ij}^{Hydrostatic}$ are negative-valued because the vertical location of the COB is far below the SWL.

The remaining hydrodynamic loads—those associated with excitation from incident waves and radiation of outgoing waves from platform motion—depend on whether flow separation occurs. For a floating platform interacting with surface waves, different formulations for the hydrodynamic loads apply to separated and nonseparated flows. For cylinders, the proper formulation—and the hydrodynamic coefficients used within each formulation—depend, among other factors, on the Keulegan-Carpenter number, *K*, and the oscillatory Reynolds number, *Re*, defined as [3]

$$K = \frac{VT}{D} \quad (4\text{-}4)$$

and

$$Re = \frac{VD}{\nu}, \quad (4\text{-}5)$$

where *D* is the cylinder diameter, *v* is the kinematic viscosity of the fluid, *T* is the wave period, and *V* is the amplitude of the fluid velocity normal to the cylinder. The diameter to wavelength ratio, D/λ, is also an important factor that determines the proper formulation. For linear regular (i.e., periodic) waves, the wavelength and (depth-dependent) wave velocity amplitude are related to the wave period and the wave height (i.e., twice the wave amplitude), *H*, by [3]

$$V = \frac{\pi H}{T} \frac{\cosh\left[k\left(Z+h\right)\right]}{\sinh\left(kh\right)} \quad (4\text{-}6)$$

and

$$\lambda = \frac{2\pi}{k}, \quad (4\text{-}7)$$

where *Z* is the local depth (negative in value), *h* is the water depth (positive in value), and *k* is the wave number, which, itself, is related to the wave period through the implicit dispersion relationship [3]:

$$k\,tanh(kh) = \frac{4\pi^2}{gT^2}\,. \tag{4-8}$$

The water depth is taken to be 320 m. From the external geometry of the floating platform and the periodic sea states defined in Table 4-1 (from 1 = mild to 8 = extreme sea state), then, the Keulegan-Carpenter number, oscillatory Reynolds number, and diameter to wavelength ratio are presented in Figure 4-1 as function of depth (Z) along the spar.

Table 4-1. Periodic Sea State Definitions

Sea State	T (s)	H (m)
1	2.0	0.09
2	4.8	0.67
3	6.5	1.40
4	8.1	2.44
5	9.7	3.66
6	11.3	5.49
7	13.6	9.14
8	17.0	15.24

The upper and middle charts in Figure 4-1 show that, for the OC3-Hywind spar-buoy, the Keulegan-Carpenter and oscillatory Reynolds numbers increase with increasing severity in the wave conditions and decrease with depth along the spar. Flow separation occurs when the Keulegan-Carpenter number exceeds 2. For values lower than 2, potential-flow theory applies. Consequently, potential-flow theory applies all along the spar in all but the most extreme wave conditions, where separation will occur along the upper portions of the platform. The bottom chart in Figure 4-1 shows that, for the OC3-Hywind spar-buoy, the diameter to wavelength ratio decreases with increasing severity of the wave conditions and is lower above the tapered region. Diffraction effects are important when this ratio exceeds 0.2 and are unimportant for smaller ratios. Consequently, diffraction effects are only important in the spar in mild wave conditions, where the hydrodynamic loads are small anyway.

In view of the validity of potential-flow theory across many conditions, the linear potential-flow problem was solved using the WAMIT computer program [10]. WAMIT uses a three-dimensional numerical-panel method in the frequency domain to solve the linearized potential-flow hydrodynamic radiation and diffraction problems for the interaction of surface waves with offshore platforms of arbitrary geometry. The solution to the radiation problem, which considers the hydrodynamic loads on the platform associated with oscillation of the platform in its various modes of motion (of which radiates outgoing waves), is given in terms of oscillation-frequency-dependent hydrodynamic-added-mass and -damping matrices, A_{ij} and B_{ij} respectively. The solution to the diffraction problem, which considers the hydrodynamic loads on the platform associated with excitation from incident waves, is given in terms of the wave-frequency- and -direction-dependent hydrodynamic-wave-excitation vector, X_i. Whereas A_{ij} and B_{ij} are real-valued, X_i is complex-valued, with the magnitude determining the load normalized per unit wave amplitude and the phase determining the lag between the wave elevation and load. The subscripts here are consistent with those of $C_{ij}^{Hydrostatic}$ discussed earlier and, as before, the loads

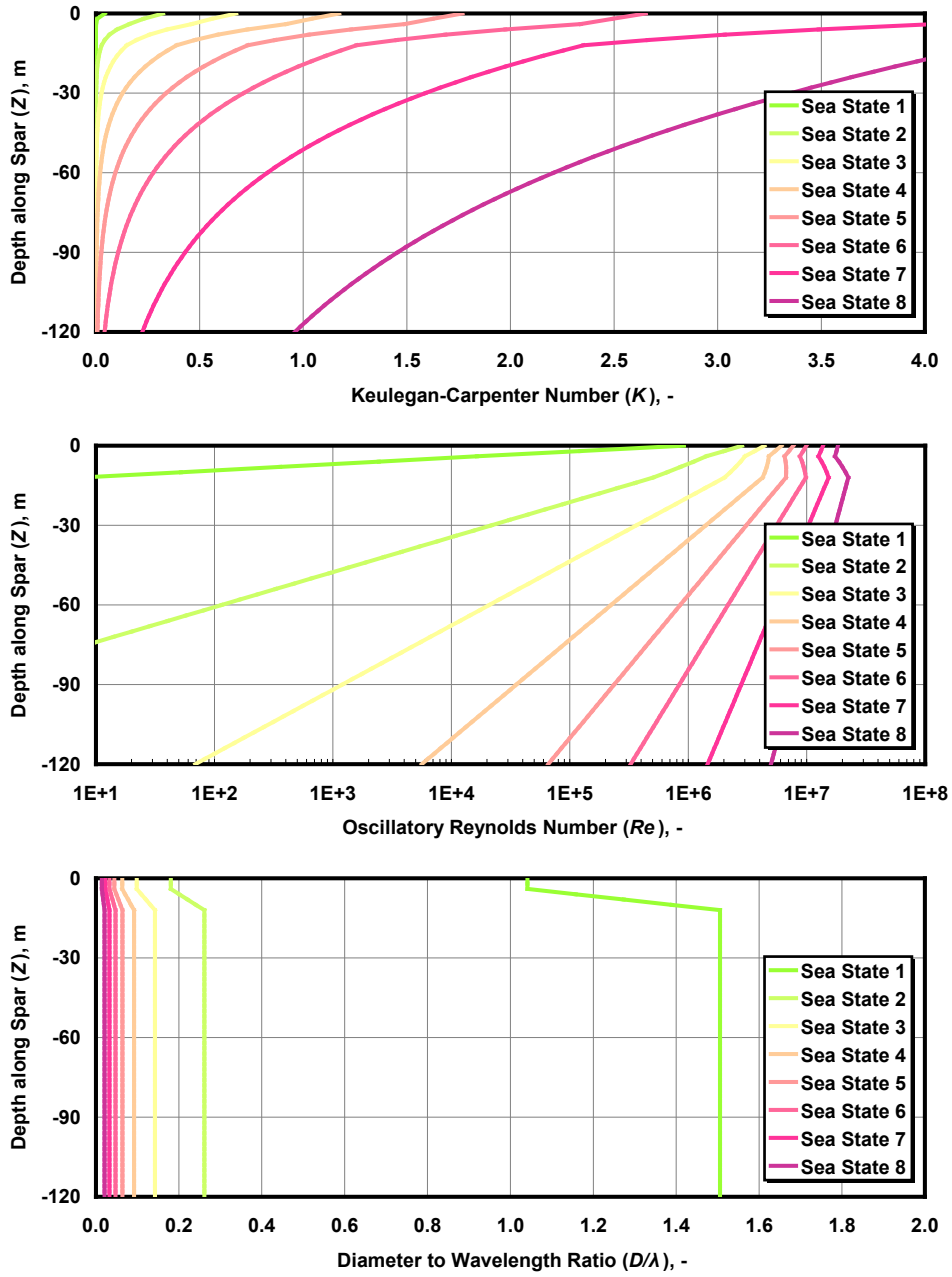

Figure 4-1. Dimensionless Parameters for the OC3-Hywind spar

are positive in the direction of positive motion. Reference [5] provides more information on potential-flow theory as it relates to floating platforms.

In WAMIT, I modeled the OC3-Hywind spar-buoy with two geometric planes of symmetry with 3,900 rectangular panels within a quarter of the body. Figure 4-2 shows the panel mesh with both symmetries. To improve the accuracy of the WAMIT results, I chose to override three default settings, choosing instead to (1) integrate the logarithmic singularity analytically, (2) solve the linear system of equations using a direct solver, and (3) remove the effects of irregular frequencies by manually paneling the free surface. These settings were necessary because

subsequent analysis required high-frequency output. The spar was analyzed in its undisplaced position (consistent with linear theory) and with finite water depth (320 m).

The magnitude and phase of the hydrodynamic-wave-excitation vector from the linear diffraction problem are shown as a function of wave frequency in Figure 4-3 for incident waves propagating along the positive *X*-axis. For these waves, the loads in the direction of the sway, roll, and yaw DOFs are zero due to the symmetries of the spar. The magnitudes of the force and moment in the direction of the surge and pitch DOFs reach a peak just above and below a wave frequency of 0.5 rad/s, respectively. At higher wave frequencies (smaller wavelengths), diffraction effects become important and the loads drop. The heave force reverses sign at about 0.25 rad/s, reaches a peak just above 0.5 rad/s, and then drops in magnitude at higher wave frequencies.

The hydrodynamic-added-mass and -damping matrices from the linear radiation problem for all six rigid-body modes of motion of the platform are shown as a function of oscillation frequency in Figure 4-4. Only the upper triangular matrix elements are shown because the hydrodynamic-added-mass and -damping matrices are symmetric in the absence of forward speed. Also, because of the spar's symmetries, the surge-surge elements of the frequency-dependent added-mass and damping matrices, A_{11} and B_{11}, are identical to the sway-sway elements, A_{22} and B_{22}. Likewise, the roll-roll elements, A_{44} and B_{44}, are identical to the pitch-pitch elements, A_{55} and B_{55}. Other matrix elements not shown are zero-valued.

As shown in Figure 4-4, the added mass of the platform varies little across oscillation frequency. The zero- and infinite-frequency limits of all elements of the damping matrix are zero (not all shown), as required by theory, and peak out at some intermediate frequency. But the values of the damping in the moment-rotation, force-rotation, and

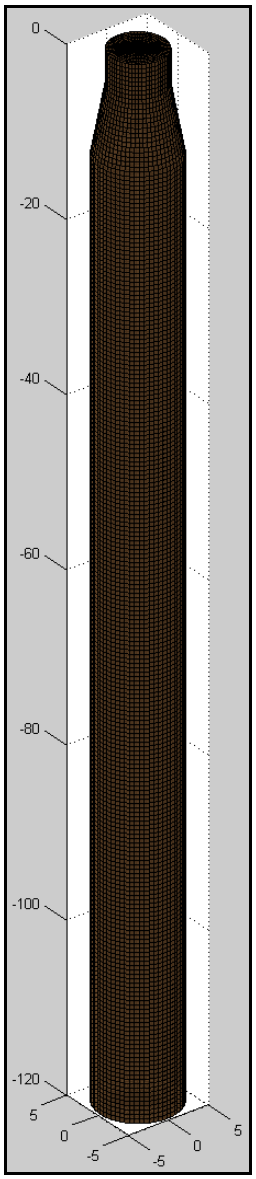

Figure 4-2. Panel mesh of the OC3-Hywind spar used within WAMIT

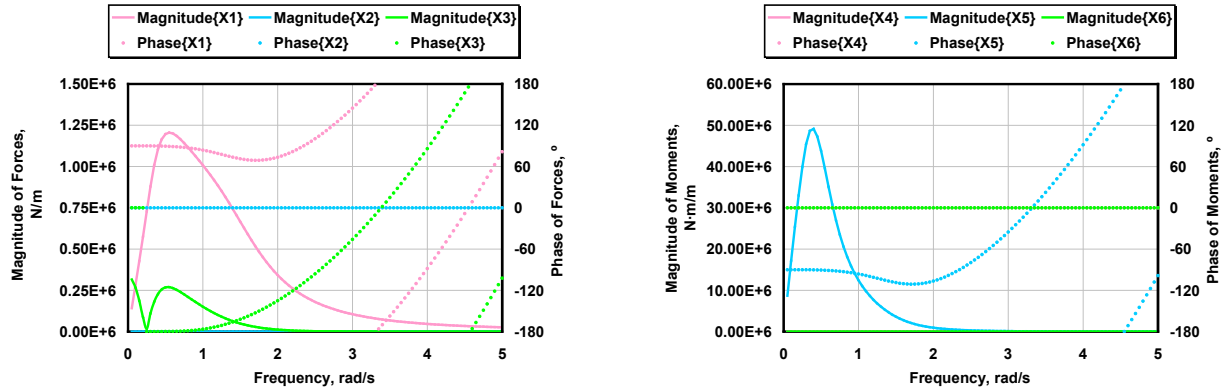

Figure 4-3. Hydrodynamic wave excitation per unit amplitude for the OC3-Hywind spar

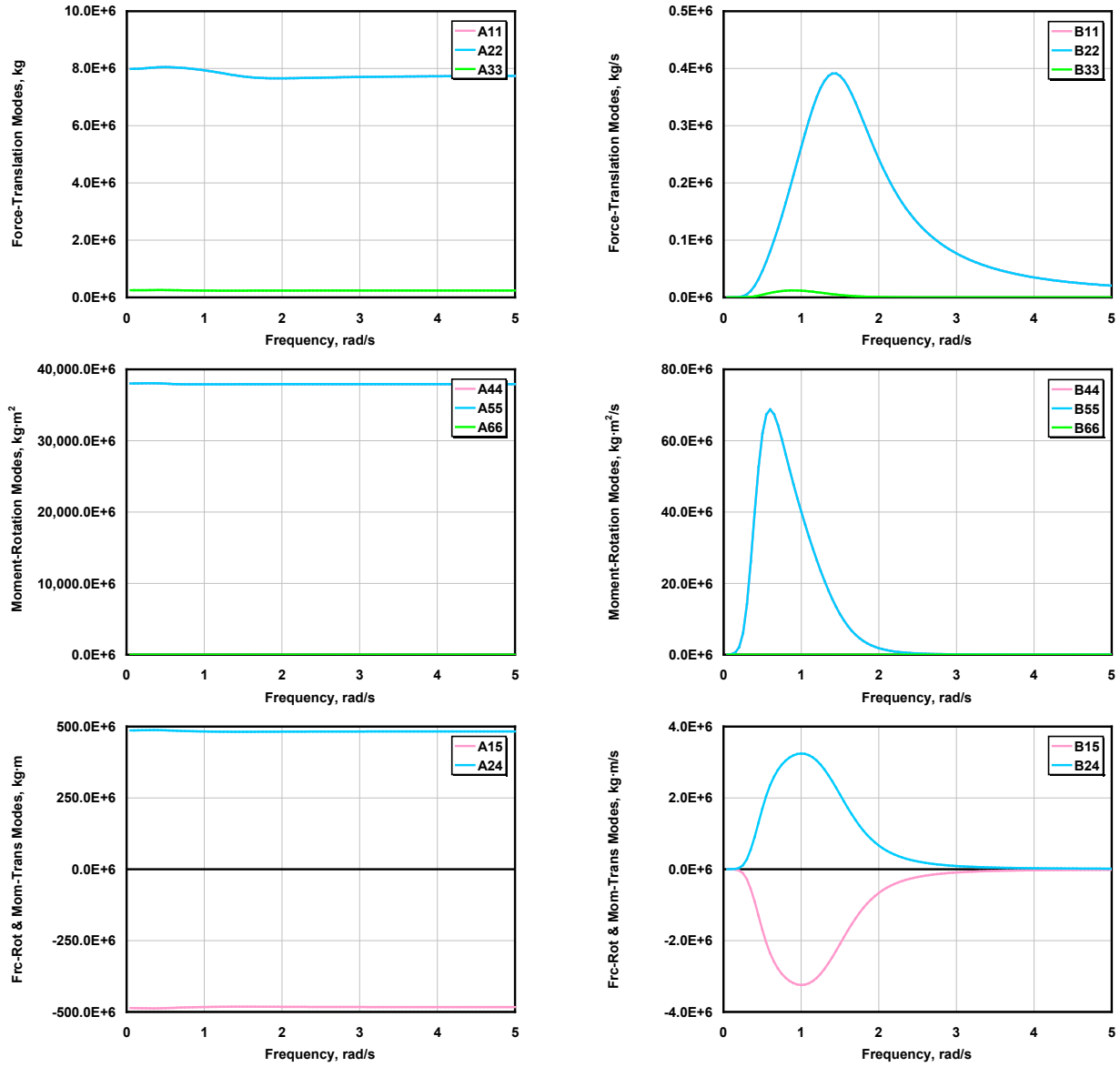

Figure 4-4. Hydrodynamic added mass and damping for the OC3-Hywind spar

moment-translation modes are considerably smaller than those of the added-mass, which imply that the linear radiation damping, and associated memory effects in the time domain, are also small in those modes. Only in the force-translation modes may the linear radiation damping and memory effect be important.

The linear memory effect is captured within time-domain hydrodynamics models through the time-convolution of the radiation impulse-response functions (i.e., the wave-radiation-retardation kernel), K_{ij}, with the platform velocities. The memory effect captures the hydrodynamic load on the platform that persists from the outgoing free-surface waves (which induce a pressure field within the fluid domain) radiated-away by platform motion. The radiation impulse-response functions can be found from the cosine transform of the frequency-dependent hydrodynamic damping matrix. The results of this computation, as performed within WAMIT's frequency-to-time (F2T) conversion utility, are shown in Figure 4-5. As before, only the upper triangular

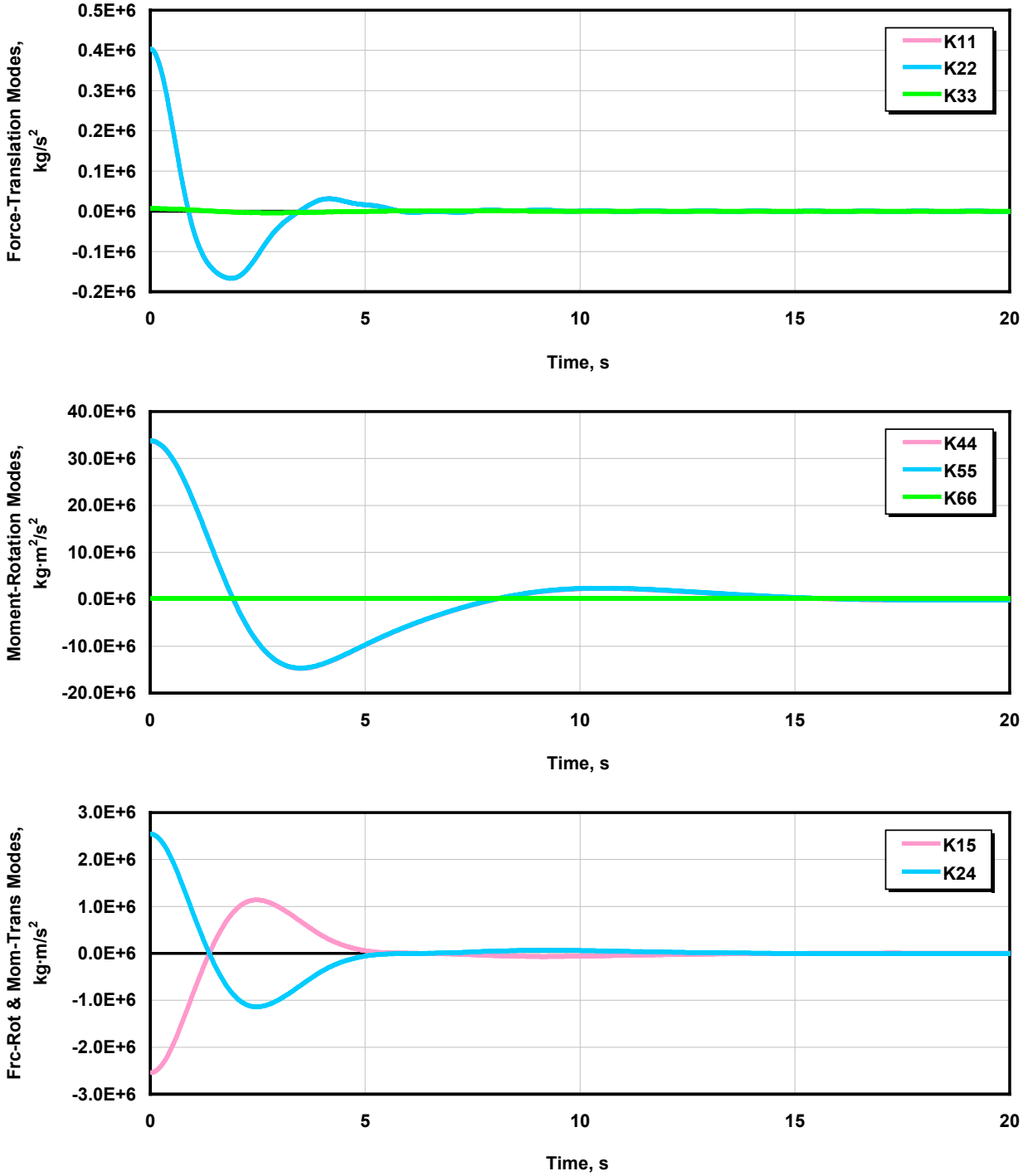

Figure 4-5. Radiation impulse-response functions for the OC3-Hywind spar

matrix elements of the symmetric K_{ij} matrix are shown, and because of the spar's symmetries, the surge-surge elements, K_{11}, are identical to the sway-sway elements, K_{22}, and the roll-roll elements, K_{44}, are identical to the pitch-pitch elements, K_{55}. Most of the response—and linear radiation damping—decays to zero after about 20 s even for the force-translation modes that may not be negligible. Reference [5] provides more information on radiation theory.

The second-order potential-flow solution, which includes mean-drift, slow-drift, and sum-frequency excitation, and higher-order solutions, were not solved and are assumed to be negligible for the OC3-Hywind spar.

In severe sea conditions, the hydrodynamic loads from linear potential-flow theory must be augmented with the loads brought about by flow separation. Moreover, many wind turbine dynamics codes cannot model hydrodynamics per linear potential-flow theory. To address these situations, a simplified hydrodynamics model using Morison's formulation is presented next.

The popular hydrodynamic formulation used in the analysis of fixed-bottom support structures for offshore wind turbines—Morison's formulation—is applicable for calculating the hydrodynamic loads on cylindrical structures when (1) the effects of diffraction are negligible, (2), radiation damping is negligible, and (3) flow separation may occur. The relative form of Morison's equation accounts for the loading from incident-wave-induced excitation, radiation-induced added mass, and flow-separation-induced viscous drag in the directions of the surge, sway, roll, and pitch DOFs. Hydrodynamic heave forces are neglected (and hydrodynamic yaw moments are zero for cylindrical structures). From the results presented above, then, Morison's equation is valid for the OC3-Hywind spar in most conditions because (1) diffraction effects are negligible in moderate to severe sea states, (2) radiation damping in most modes of motion is small, and (3) flow separation will occur in severe sea states along the upper regions of the spar.

The added-mass coefficient, C_A, to be used in Morison's equation was selected so as to give equivalent added mass in surge regardless of whether one applies linear potential-flow theory or Morison's equation within OC3. If it is assumed that C_A is independent of depth and that the motion is of low-frequency, this implies that $C_A \rho V_0$ (from Morison's equation) must equal the zero-frequency limit of A_{11} (from the potential-flow solution of Figure 4-4). By this equivalency, then, the added mass coefficient for the OC3-Hywind spar is taken to be 0.969954. Also, Figure 4-1 shows that the OC3-Hywind spar experiences oscillatory Reynolds numbers exceeding 10^5 in most conditions of importance—that is, in moderate to severe sea conditions. Thus, the viscous-drag coefficient, C_D, is taken to be 0.6 (which is the typical coefficient for a cylinder at high oscillatory Reynolds numbers as shown in Figure 6.36 on page 254 of Ref. [3]). For the OC3 project, these coefficients should be applied in all simulations for those analysts who wish to apply Morison's equation. When Morison's equation is applied, however, the hydrodynamic heave forces must be added separately. For a deep-drafted spar, the heave force can be approximated as the change in buoyancy brought about by direct integration of the hydrostatic pressure dependent on the time-varying wave elevation (as was done by many modelers in OC3 Phase III).

For those OC3 analysts who choose to apply linear potential-flow theory, the hydrodynamic calculations in the directions of the surge, sway, roll, and pitch DOFs should be augmented with the nonlinear viscous-drag term from the relative form of Morison's equation. The same viscous-drag coefficient discussed above ($C_D = 0.6$) should be used. This augmentation to linear potential-flow theory is needed to obtain suitable hydrodynamic damping in severe sea conditions, which in the OC3-Hywind spar is dominated by (nonlinear) flow separation.

According to StatoilHydro, the linear radiation damping (from potential-flow theory, which is small) and the nonlinear viscous-drag (from the relative form of Morison's formulation), when

summed, do not capture all of the hydrodynamic damping for the motions of the real Hywind platform. As such, StatoilHydro recommended that the hydrodynamics models for the OC3-Hywind system, as described above, be augmented with additional linear damping. To determine the amount of additional damping required in the OC3-Hywind system, StatoilHydro provided still-water free-decay responses for all six rigid-body modes-of-motion of the Hywind system. These responses were used as target responses for the OC3-Hywind system. A model of the OC3-Hywind system was assembled in the FAST code [6], from which still-water free-decay responses were simulated with and without additional linear damping. (FAST includes a hydrodynamics model that was needed to make these calculations. This hydrodynamics model consists of linear potential-flow theory in the time domain augmented with the nonlinear viscous-drag term from the relative form of Morison's equation [5]. The additional linear damping was added on top of these hydrodynamic loads.) Additional linear damping of 100,000 N/(m/s) was needed for surge and sway motions, 130,000 N/(m/s) was needed for heave motions, and 13,000,000 Nm/(rad/s) was needed for yaw motions to match the free-decay responses supplied by StatoilHydro. (No additional damping was needed for roll and pitch motions.) This damping applies to the platform motions directly and not to the relative motion between the platform and wave particle velocities. In equation form:

$$F_i^{Additional\ Damping}\left(\dot{q}\right) = -B_{ij}^{Linear}\dot{q}_j\,, \tag{4-9}$$

with:

$$B_{ij}^{Linear} = \begin{bmatrix} 100{,}000\ N/(m/s) & 0 & 0 & 0 & 0 & 0 \\ 0 & 100{,}000\ N/(m/s) & 0 & 0 & 0 & 0 \\ 0 & 0 & 130{,}000\ N/(m/s) & 0 & 0 & 0 \\ 0 & 0 & 0 & 0 & 0 & 0 \\ 0 & 0 & 0 & 0 & 0 & 0 \\ 0 & 0 & 0 & 0 & 0 & 13{,}000{,}000\ Nm/(rad/s) \end{bmatrix}, \tag{4-10}$$

where B_{ij}^{Linear} is the (i,j) component of the additional linear damping matrix, and $\dot{q}_j$ is the first time derivative of the j^{th} platform DOF. (Without the subscript, $\dot{q}$ represents the set of first time derivatives of the platform DOFs. $F_i^{Additional\ Damping}$ depends on $\dot{q}$ as indicated.) In Eq. (4-9), subscripts i and j range from 1 to 6; one for each platform DOF (1 = surge, 2 = sway, 3 = heave, 4 = roll, 5 = pitch, 6 = yaw). Einstein notation is used here, in which it is implied that when the same subscript appears in multiple variables in a single term, there is a sum of all of the possible terms. The loads are positive in the direction of positive motion of DOF i.

For the OC3 project, all analysts should augment their hydrodynamics models with this additional damping in all simulations.

Table 4-2 summarizes the hydrodynamic properties (except the linear potential-flow solution) discussed in this section.

Table 4-2. Floating Platform Hydrodynamic Properties

Water Density (ρ)	1,025 kg/m^3
Water Depth (h)	320 m
Buoyancy Force in Undisplaced Position ($\rho g V_0$)	80,708,100 N
Hydrostatic Restoring in Heave ($C_{33}^{Hydrostatic}$)	332,941 N/m
Hydrostatic Restoring in Roll ($C_{44}^{Hydrostatic}$)	-4,999,180,000 Nm/rad
Hydrostatic Restoring in Pitch ($C_{55}^{Hydrostatic}$)	-4,999,180,000 Nm/rad
Added-Mass Coefficient (C_A in Morison's Equation)	0.969954
Viscous-Drag Coefficient (C_D in Morison's Equation)	0.6
Additional Linear Damping in Surge (B_{11}^{Linear})	100,000 N/(m/s)
Additional Linear Damping in Sway (B_{22}^{Linear})	100,000 N/(m/s)
Additional Linear Damping in Heave (B_{33}^{Linear})	130,000 N/(m/s)
Additional Linear Damping in Yaw (B_{66}^{Linear})	13,000,000 Nm/(rad/s)

5 Mooring System Properties

To prevent it from drifting, StatoilHydro's Hywind platform is moored by a system of three catenary lines. The lines attach to the platform via a so-called "crowfoot" (delta connection) to increase the moorings' yaw stiffness. Also, each line consists of multiple segments of varying properties and a clump weight.

In order to simplify the analysis of the mooring system within the OC3 project, however, only the specifications of an effective system are presented for the OC3-Hywind system. Three simplifications are made. First, the delta connection is eliminated, which requires that the mooring system be augmented with a yaw spring to achieve the proper overall yaw stiffness. Second, each of the multisegment lines is replaced with an equivalent homogenous line, with properties derived as the weighted-average values of the mass, weight, and stiffness (weighted based on the unstretched lengths of each segment). Third, all mooring system damping, including the hydrodynamic drag and line-to-seabed drag, is neglected. Please note that these three simplifications are acceptable for static analysis, but may not be appropriate in all dynamical conditions. From these simplifications, the fairleads (body-fixed locations where the mooring lines attach to the platform) are located at a depth of 70.0 m below the SWL and at a radius of 5.2 m from the platform centerline. The anchors (fixed to the inertia frame) are located at a (water) depth of 320 m below the SWL and at a radius of 853.87 m from the platform centerline. One of the lines is directed along the positive *X*-axis (in the *XZ*-plane). The two remaining lines are distributed uniformly around the platform, such that each line, fairlead, and anchor is 120º apart when looking from above. These properties are relative to the undisplaced position of the platform. Each of the 3 lines has an unstretched length of 902.2 m, a diameter of 0.09 m, an equivalent mass per unit length of 77.7066 kg/m, an equivalent apparent weight in fluid per unit length of 698.094 N/m, and an equivalent extensional stiffness of 384,243,000 N. The additional yaw spring has a stiffness of 98,340,000 Nm/rad. Table 5-1 summarizes these properties.

Table 5-1. Mooring System Properties

Number of Mooring Lines	3
Angle Between Adjacent Lines	120º
Depth to Anchors Below SWL (Water Depth)	320 m
Depth to Fairleads Below SWL	70.0 m
Radius to Anchors from Platform Centerline	853.87 m
Radius to Fairleads from Platform Centerline	5.2 m
Unstretched Mooring Line Length	902.2 m
Mooring Line Diameter	0.09 m
Equivalent Mooring Line Mass Density	77.7066 kg/m
Equivalent Mooring Line Weight in Water	698.094 N/m
Equivalent Mooring Line Extensional Stiffness	384,243,000 N
Additional Yaw Spring Stiffness	98,340,000 Nm/rad

Many wind turbine dynamics codes cannot model the individual mooring lines. For these codes, three simplified models are presented. The first is a linearized model of the complete mooring system. The second is a nonlinear model of the complete mooring system. The third is a

nonlinear model of an individual mooring line. Please note that these simplified models must also be augmented with the additional yaw spring specified above (the simplified models presented below do not include the effects of the additional yaw spring).

If the mooring system compliance were inherently linear and mooring inertia and damping were ignored, as assumed in the first simplified model, the total load on the support platform from the contribution of all mooring lines, F_i^{Lines}, would be

$$F_i^{Lines}\left(q\right) = F_i^{Lines,0} - C_{ij}^{Lines} q_j \,, \tag{5-1}$$

where $F_i^{Lines,0}$ is the i^{th} component of the total mooring system load acting on the support platform in its undisplaced position, C_{ij}^{Lines} is the (i,j) component of the linearized restoring matrix from all mooring lines, and q_j is the j^{th} platform DOF. (Without the subscript, q represents the set of platform DOFs. F_i^{Lines} depends on q as indicated.) For catenary mooring lines, $F_i^{Lines,0}$ represents the pre-tension at the fairleads from the weight of the mooring lines not resting on the seafloor in water. C_{ij}^{Lines} is the combined result of the elastic stiffness of the mooring lines and the effective geometric stiffness brought about by the weight of the lines in water, depending on the layout of the mooring system. In Eq. (5-1), subscripts i and j range from 1 to 6; one for each platform DOF (1 = surge, 2 = sway, 3 = heave, 4 = roll, 5 = pitch, 6 = yaw). Einstein notation is used here, in which it is implied that when the same subscript appears in multiple variables in a single term, there is a sum of all of the possible terms. The loads are positive in the direction of positive motion of DOF i.

For the mooring system considered here, $F_i^{Lines,0}$ and C_{ij}^{Lines} were calculated by performing a linearization analysis in the FAST code [6] about the undisplaced position of the platform (i.e., about the linearization point where all DOF displacements are zero-valued). (FAST includes a mooring system model [5] that was needed to make these calculations.) The linearization analysis involves independently perturbing the platform DOFs and measuring the resulting variations in mooring loads. Within FAST, the partial derivatives are computed using the central-difference-perturbation numerical technique. The results are as follows:

$$F_i^{Lines,0} = \begin{Bmatrix} 0 \\ 0 \\ -1{,}607{,}000\ N \\ 0 \\ 0 \\ 0 \end{Bmatrix} \tag{5-2}$$

and

$$C_{ij}^{Lines} = \begin{bmatrix} 41{,}180\ N/m & 0 & 0 & 0 & -2{,}821{,}000\ N/rad & 0 \\ 0 & 41{,}180\ N/m & 0 & 2{,}821{,}000\ N/rad & 0 & 0 \\ 0 & 0 & 11{,}940\ N/m & 0 & 0 & 0 \\ 0 & 2{,}816{,}000\ Nm/m & 0 & 311{,}100{,}000\ Nm/rad & 0 & 0 \\ -2{,}816{,}000\ Nm/m & 0 & 0 & 0 & 311{,}100{,}000\ Nm/rad & 0 \\ 0 & 0 & 0 & 0 & 0 & 11{,}560{,}000\ Nm/rad \end{bmatrix} \quad (5\text{-}3)$$

Of course, the linear model is only valid for small displacements about the linearization point. For larger displacements, it is important to capture the nonlinear relationships between load and displacement, as provided in the second simplified model. In general, all six components of F^{Lines} depend nonlinearly on all six displacements of q. (Without the subscript, F^{Lines} represents the set of mooring system loads, including three forces and three moments.) For the mooring system considered here, these load-displacement relationships were found numerically using the FAST code [6] by considering discrete combinations of the displacements. The surge and sway displacements (q_1 and q_2) were varied from −36 to 36 m in steps of 6 m. The heave displacement (q_3) was varied from−12 to 12 m in steps of 4 m. The roll and pitch displacements (q_4 and q_5) were varied from −10º to 10º in steps of 2º. The yaw displacement (q_6) was varied from −20º to 20º in steps of 4º. All six components of F^{Lines} were calculated for every combination of these displacements, for a total of (13 × 13 × 7 × 11 × 11 × 11 =) 1,574,573 discrete combinations. The upper and lower bounds in these variations were determined by estimating the anticipated displacement limits through a handful of time-domain simulations of the full system that included varying wind and wave conditions and operational status of the wind turbine. The step sizes were chosen so as to produce reasonable resolution in the nonlinear response at a minimal computational cost. All of the data—that is, all six components of F^{Lines} dependent on all six displacements of q—was written to a text file: "MooringSystemFD.txt".

Figure 5-1 shows the load-displacement relationships for the OC3-Hywind mooring system when each platform DOF is varied independently with all other displacements zero-valued [i.e., Figure 5-1 presents a sample of one-dimensional (1D) load-displacement relationships]. The relationships include some interesting asymmetries, which result from the nonlinear behavior of the three-point mooring system. Whereas the loads are either symmetric or anti-symmetric about zero for the sway (q_2) and roll (q_4) displacements, the loads are asymmetric about zero for the surge (q_1) and pitch (q_5) displacements. For the surge and pitch displacements, the mooring system stiffens up—and the surge forces, heave forces, and pitching moments increase nonlinearly—when the fairleads translate along the –*X*-axis. This asymmetry also induces surge forces and pitching moments when the fairleads translate along the *Y*-axis due to sway and roll displacements. Also, the heave forces change with all displacements because these displacements cause more line to lift off of—or allow more line to settle on—the seabed. The slopes of these load-displacement relationships about zero-displacement are consistent with the elements of the linearized restoring matrix, C_{ij}^{Lines}, presented above.

Figure 5-2 shows the nonlinear relationships for the surge forces and pitching moments associated with surge and pitch displacements and the sway forces and roll moments associated with sway and roll displacements with all other displacements zero-valued [i.e., Figure 5-2 presents a sample of two-dimensional (2D) load-displacement relationships]. The combinations of surge and pitch displacements and sway and roll displacements were plotted because those displacements are often correlated. The data in Figure 5-2 shows that, unless large loads are

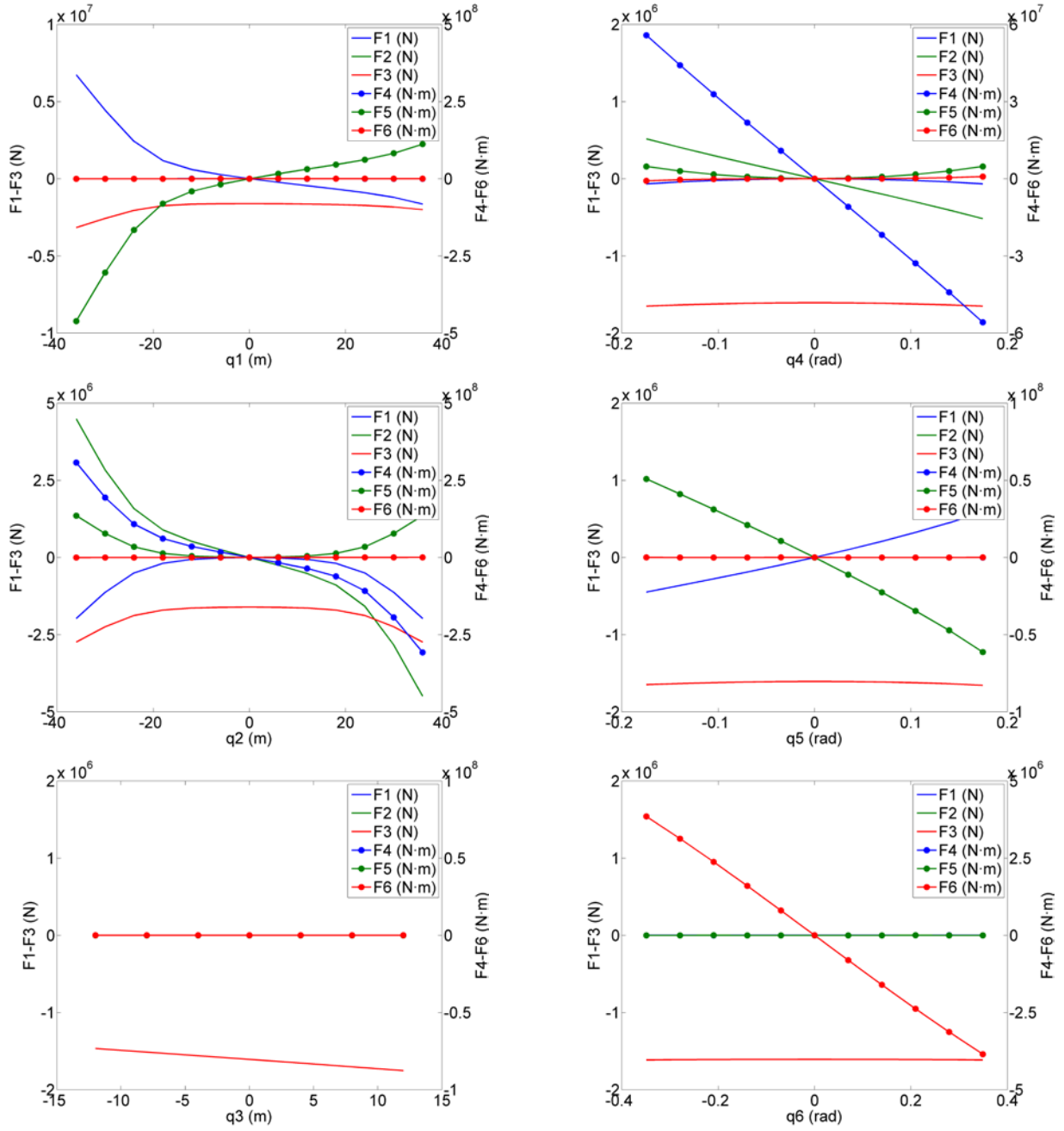

Figure 5-1. Load-displacement relationships for the OC3-Hywind mooring system in 1D

applied to the platform to react with the rapidly increasing mooring loads, as the platform translates positively (or negatively) in surge, it will tend to pitch positively (or negatively) accordingly and as the platform translates positively (or negatively) in sway, it will tend to roll negatively (or positively) accordingly. The data in Figure 5-2 also shows the asymmetry about zero-displacement between translations of the fairlead along the *X*- and *Y*-axes (due to surge and pitch displacements and sway and roll displacements, respectively) just as the results of Figure 5-1 showed. The data in Figure 5-2 are also consistent with the results of Figure 5-1, as some of the results of Figure 5-1 are slices through the data of Figure 5-2 when one of the displacements in Figure 5-2 is zero-valued.

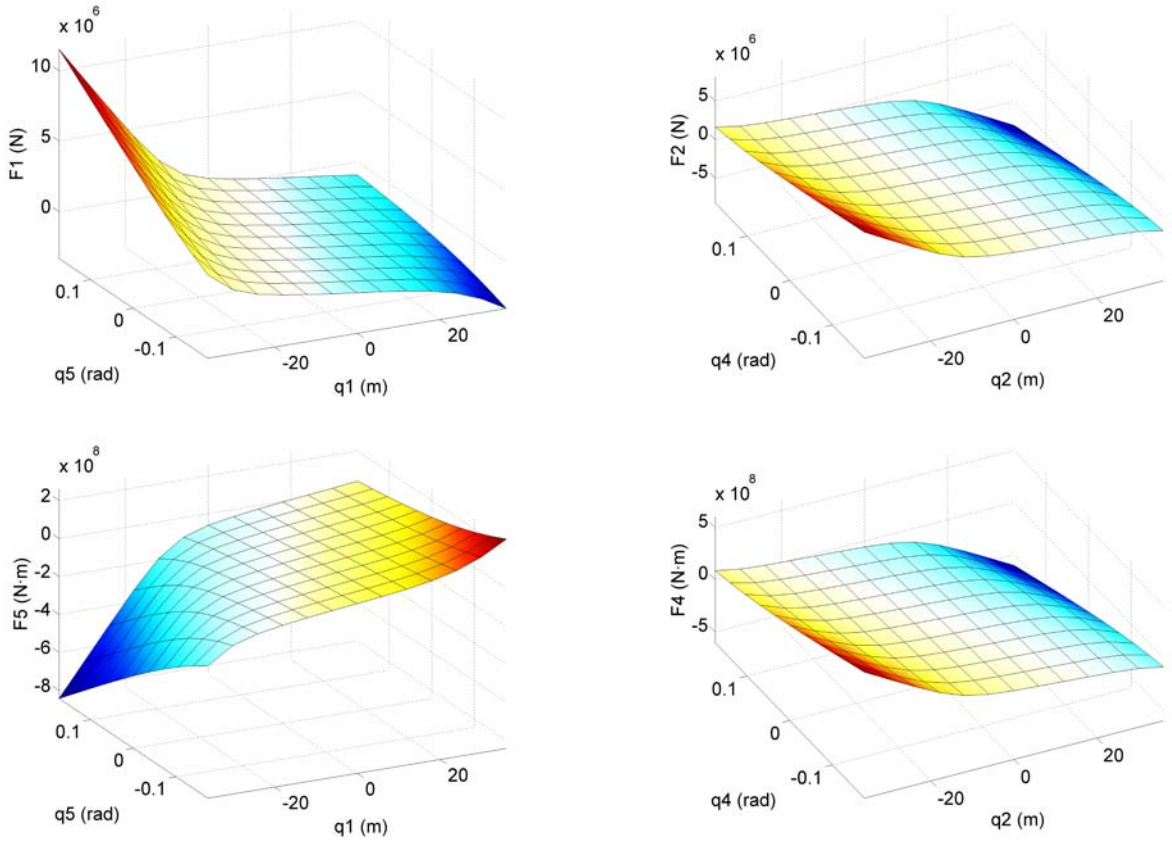

Figure 5-2. Load-displacement relationships for the OC3-Hywind mooring system in 2D

The two simplified mooring system models presented above only capture the total load acting on the support platform from the complete mooring system; no information is given regarding the reactions within each individual mooring line. The third simplified mooring system model addresses this limitation by giving the load-displacement relationship of an individual mooring line. The model is presented in the output format of the MIMOSA mooring analysis software [2], which gives the qausi-static reactions of an individual mooring line as a function of the horizontal distance between the fairlead and anchor. The vertical distance between the fairlead and anchor is fixed at (320 m – 70 m) = 250 m in this model; 250 m is equal to the vertical distance between the fairlead and anchor when the platform is undisplaced in pitch, roll and heave. In the nomenclature of MIMOSA format, "DISTANCE" is the horizontal distance between the fairlead and anchor. "TENSION" is the total (vector combination of the horizontal and vertical tensions) in the mooring line at the fairlead. "H.TENSION" is the horizontal component of this fairlead tension. "SUSPL" is the distance along the line from the fairlead to the equivalent point on the unstretched mooring line where the point on the stretched mooring line first touches the seabed. "TEN.ANCH" is the total (vector combination of the horizontal and vertical tensions) in the mooring line at the anchor.

For the OC3-Hywind mooring lines considered here, this model was derived numerically using the FAST code [6] by considering a range of discrete horizontal distances for one of the three identical mooring lines. That is, DISTANCE was varied from 653.0 m to 902.5 m in steps of 0.5 m, for a total of 500 discrete steps. The upper and lower bounds were determined by choosing

limits far beyond the likely distances that will be covered when the full system model is run in time-domain simulations. The step size was chosen so as to produce reasonable resolution in the nonlinear response at a minimal computational cost. All of the data—that is, TENSION, H.TENSION, SUSPL, and TEN.ANCH dependent on DISTANCE—was written to a text file: "MooringLineFD.txt".

Figure 5-3 shows the data. The largest nonlinearities in the mooring line tensions occur for horizontal distances, DISTANCE, between 800 – 870 m. Below 858.5 m of DISTANCE, a portion of the mooring line rests on the seabed, such that SUSPL is less than the total unstretched length of the mooring line, 902.2 m. In this situation, the anchor tension, TEN.ANCH, is purely horizontal and—by a balance of external forces on the mooring line that has no drag—is equal to the horizontal tension at the fairlead, H.TENSION. The total tension at the fairlead, TENSION, is larger than H.TENSION because it includes a vertical component combined from the elastic stretching and the weight in water of the mooring line not resting on the seabed. For DISTANCE larger than 858.5 m, no portion of the mooring line rests on the seabed, such that SUSPL equals 902.2 m and the anchor tension includes a nonzero vertical component, which causes TEN.ANCH to exceed the value of H.TENSION. All tensions rise dramatically as the mooring line gets more and more taut.

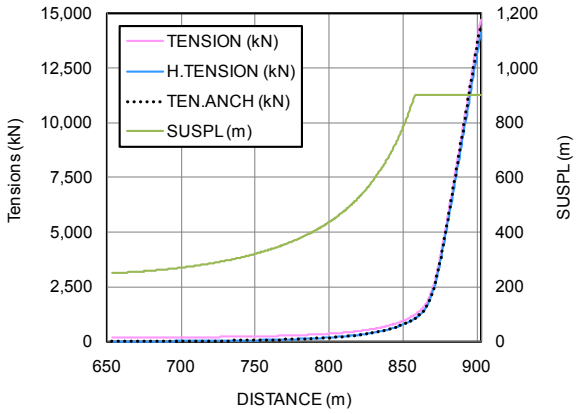

Figure 5-3. Load-displacement relationships for one OC3-Hywind mooring line

6 Control System Properties

The NREL 5-MW wind turbine uses a conventional variable-speed, variable blade-pitch-to-feather control system [7]. A consequence of conventional pitch-to-feather control of wind turbines, though, is that steady-state rotor thrust is reduced with increasing wind speed above rated. As pointed out by Nielsen, Hanson, and Skaare in Ref. [11, p. 673], "this effect may introduce negative damping in the system that may lead to large resonant motions of [a] floating wind turbine." As the analyses of Refs. [5,9,11,12] have demonstrated, it is important that the damping of the platform-pitch mode be positive and kept as large as possible.

Larsen and Hansen [9] and I [5] have presented modifications to conventional wind turbine control systems that aim to eliminate the potential for negative damping of the platform-pitch mode and improve a floating turbine system's response. Two of these modifications were applied to the original control system for the NREL 5-MW turbine (as presented in Ref. [7]) to arrive a control system that is suitable for when the turbine is installed on the OC3-Hywind spar-buoy.

The first modification was a reduction of gains in the blade-pitch-to-feather control system. In an idealized PI-based blade-pitch controller, the rotor azimuth responds as a second-order system with a natural frequency and damping ratio [4]. To maintain a reasonable relationship between the proportional and integral gains in this control system, the gains were reduced by choosing a smaller controller-response natural frequency while preserving the recommended controller damping ratio. The value of this frequency as recommended in Ref. [4], and the value selected for the baseline control system, of 0.6 rad/s [7] is above the platform-pitch natural frequency of about 0.21 rad/s. This relationship between frequencies has the potential to introduce negative damping of the platform-pitch mode. Larsen and Hanson [9] found that the smallest controller-response natural frequency must be lower than the smallest critical support-structure natural frequency to ensure that the support-structure motions of an offshore floating wind turbine with active pitch-to-feather control remain positively damped. Reducing the controller-response natural frequency to 0.2 rad/s will ensure that it is lower than the platform-pitch natural frequency and also lower than wave-excitation frequency of most sea states. Using the properties for the NREL 5-MW wind turbine from Ref. [7], this frequency and the damping ratio used prior were used to derive the reduced proportional gain at minimum blade-pitch setting of 0.006275604 s and the reduced integral gain at minimum blade-pitch setting of 0.0008965149. The gain-correction factor in the gain-scheduling law of the blade-pitch controller is unaffected by this change.

The second modification was a change to the generator-torque control strategy when operating at rated power (i.e., control Region 3). That is, the control law in Region 3 was changed from a constant generator power to a constant generator-torque control region. The constant generator torque is set to the rated torque of 43,093.55 N•m. With this change, the generator-torque controller does not introduce negative damping in the rotor-speed response (which must be compensated by the blade-pitch controller), and so, reduces the rotor-speed excursions that are exaggerated by the reduction in gains in the blade-pitch controller. This improvement, though, comes at the expense of some overloading of the generator, as power increases with rotor-speed

excursions above rated. Larson and Hanson [9] have demonstrated the effectiveness of this modification.

These modifications were incorporated into an updated version of the baseline control system dynamic link library (DLL) suitable for use with the floating system discussed in this report, which, as before, is in the style of Garrad Hassan's *BLADED* wind turbine software package [1].

Table 6-1 summarizes the updated properties of the baseline control system discussed in this section.

Table 6-1. Baseline Control System Property Modifications

Proportional Gain at Minimum Blade-Pitch Setting	0.006275604 s
Integral Gain at Minimum Blade-Pitch Setting	0.0008965149
Constant (Rated) Generator Torque in Region 3	43,093.55 N•m

References

[1] Bossanyi, E. A., *GH Bladed Version 3.6 User Manual*, 282/BR/010, Bristol, UK: Garrad Hassan and Partners Limited, December 2003.

[2] Det Norske Veritas. *MIMOSA Mooring Analysis Software*.

[3] Gudmestad, O. T., et al, *Basics of Offshore Petroleum Engineering and Development of Marine Facilities — With Emphasis on the Arctic Offshore*, Stavanger, Moscow, St. Petersburg, Trondheim, December 1998.

[4] Hansen, M. H., Hansen, A., Larsen, T. J., Φye, S., Sørensen, and Fuglsang, P., *Control Design for a Pitch-Regulated, Variable-Speed Wind Turbine*, Risø-R-1500(EN), Roskilde, Denmark: Risø National Laboratory, January 2005.

[5] Jonkman, J. M., *Dynamics Modeling and Loads Analysis of an Offshore Floating Wind Turbine*, Ph.D. Thesis, Department of Aerospace Engineering Sciences, University of Colorado, Boulder, CO, 2007; NREL/TP-500-41958, Golden, CO: National Renewable Energy Laboratory.

[6] Jonkman, J. M. and Buhl Jr., M. L. *FAST User's Guide*, NREL/EL-500-38230 (previously NREL/EL-500-29798), Golden, CO: National Renewable Energy Laboratory, August 2005.

[7] Jonkman, J., Butterfield, S., Musial, W., and Scott, G., *Definition of a 5-MW Reference Wind Turbine for Offshore System Development*, NREL/TP-500-38060, Golden, CO: National Renewable Energy Laboratory, February 2009.

[8] Kooijman, H. J. T., Lindenburg, C., Winkelaar, D., and van der Hooft, E. L., "DOWEC 6 MW Pre-Design: Aero-elastic modeling of the DOWEC 6 MW pre-design in PHATAS," *DOWEC Dutch Offshore Wind Energy Converter 1997–2003 Public Reports* [CD-ROM], DOWEC 10046_009, ECN-CX--01-135, Petten, the Netherlands: Energy Research Center of the Netherlands, September 2003.

[9] Larsen, T. J. and Hanson, T. D., "A Method to Avoid Negative Damped Low Frequent Tower Vibrations for a Floating, Pitch Controlled Wind Turbine," *Journal of Physics: Conference Series, The Second Conference on The Science of Making Torque From Wind, Copenhagen, Denmark, 28–31 August 2007*, [online journal], Vol. 75, 2007, 012073, URL: http://www.iop.org/EJ/article/1742-6596/75/1/012073/jpconf7_75_012073.pdf?request-id=SpEuhRBu3BG0xV3r2wi7Kg, [cited 28 August 2007].

[10] Lee, C. H. and Newman, J. N., *WAMIT® User Manual, Versions 6.3, 6.3PC, 6.3S, 6.3S-PC*, Chestnut Hill, MA: WAMIT, Inc., 2006.

[11] Nielsen, F. G., Hanson, T. D., and Skaare, B., "Integrated Dynamic Analysis of Floating Offshore Wind Turbines," *Proceedings of OMAE2006 25th International Conference on Offshore Mechanics and Arctic Engineering, 4–9 June 2006, Hamburg, Germany* [CD-

ROM], Houston, TX: The American Society of Mechanical Engineers (ASME International) Ocean, Offshore and Arctic Engineering (OOAE) Division, June 2006, OMAE2006-92291.

[12] Skaare, B., Hanson, T. D., and Nielsen, F. G., "Importance of Control Strategies on Fatigue Life of Floating Wind Turbines," *Proceedings of OMAE2007 26th International Conference on Offshore Mechanics and Arctic Engineering, 10–15 June 2007, San Diego, CA* [CD-ROM], Houston, TX: The American Society of Mechanical Engineers (ASME International) Ocean, Offshore and Arctic Engineering (OOAE) Division, June 2007, OMAE2007-29277.